

AuON: A Linear-time Alternative to Semi-Orthogonal Momentum Updates

Dipan Maity
 dipanai.xyz@gmail.com

September 30, 2025

Abstract

Orthogonal gradient updates have emerged as a promising direction in optimization for machine learning. However, traditional approaches such as SVD/QR decomposition incur prohibitive computational costs of $\mathcal{O}(n^3)$ and underperformed compared to well-tuned SGD with momentum, since momentum is applied only after strict orthogonalization. Recent advances, such as Muon, improve efficiency by applying momentum before orthogonalization and producing semi-orthogonal matrices via Newton–Schulz iterations, reducing complexity to $\mathcal{O}(n^2)$. Nevertheless, quadratic costs remain a bottleneck.

In this work, we study the semi-orthogonal properties of momentum-based updates and develop a method to bound momentum updates under a spectral-norm trust region, preserving directional information without requiring explicit semi-orthogonalization.

We propose **AuON** (Alternative Unit-norm momentum updates by Normalized nonlinear scaling), a linear-time optimizer that achieves strong performance without constructing semi-orthogonal matrices, while preserving structural alignment and reconditioning ill-posed updates. Our approach combines hyperbolic-cosine RMS scaling transformations with normalization, demonstrating both effectiveness and computational efficiency compared to Newton–Schulz methods. We further introduce a hybrid variant (**Hybrid-AuON**) that applies a single Newton–Schulz iteration. Experiments across vision and language benchmarks show that AuON and its hybrid variant achieve performance comparable to strong baselines such as AdamW and Muon.

Code is available at: <https://github.com/ryyzn9/AuON>

1 Introduction

”If you want to achieve extraordinary progress in AI, you should enhance the optimizer, as it fundamentally determines how models learn.”

Optimization in deep neural networks remains a central challenge, particularly due to the ill-conditioning of gradient and momentum updates. Empirically, these updates often exhibit a high condition number, with most of the energy concentrated in a few dominant directions. In practical terms, the update vectors are nearly low-rank: a handful of directions dictate the optimization trajectory while many potentially informative directions

may be suppressed. This imbalance reminds us of a squashed ball that can only roll efficiently along a single axis, ignoring other pathways that may be equally important for generalization and representation learning. One solution is to make all update directions unit length; recent work has proposed orthogonalization of gradients and momentum updates to achieve this property.

By orthogonalizing an update matrix, we effectively discard the scaling information encoded in the singular values and modify each direction to enforce perpendicularity, redistributing the update length into unit vectors along different directions. In this sense, the resulting update behaves as a *unit-norm* update in the spectral domain, emphasizing the geometric structure of the optimization landscape rather than the raw gradient magnitudes. In simple terms, orthogonalization amplifies ‘rare directions’ with small magnitude in the update but which are nevertheless important for learning. This perspective highlights how orthogonalization can prioritize exploration across all relevant directions, mitigating the dominance of a few high-energy components and facilitating more balanced learning dynamics Zhang et al. [2025]. Orthogonalized updates can therefore be interpreted as spectral descent directions, ensuring that updates explore the space more evenly-crucial for generalization and representation learning.

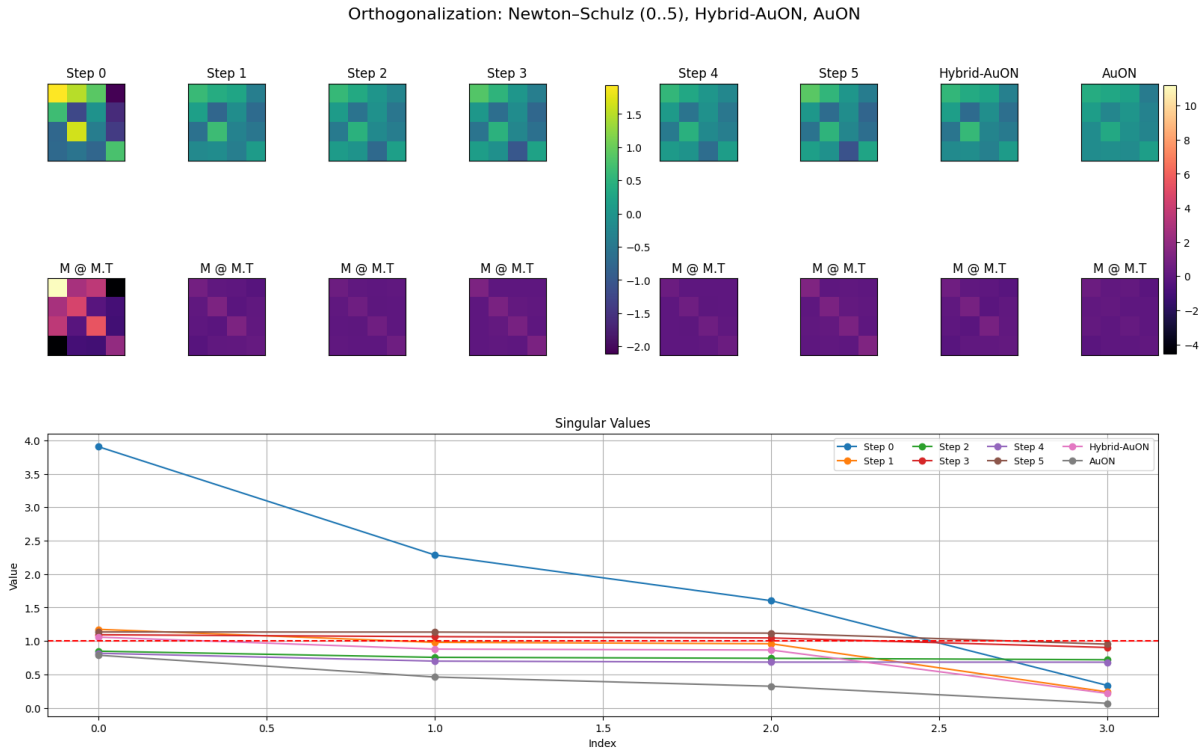


Figure 1: Visualization of the Newton–Schulz process (0.5) over 5 iterations, compared with AuON and Hybrid-AuON. The heatmaps (top) show progressive orthogonalization, with MM^T converging from a scattered structure (Step 0) to an identity-like diagonal (Step 5). The singular value plot (bottom) illustrates rapid convergence toward 1.0, confirming orthogonalization.

Tuddenham et al. [2022] proposed an approach for neural network optimization in which the gradient is first orthogonalized via singular value decomposition (SVD), followed by the application of momentum, and then the resulting momentum term is used

as the update. They refer to this method as Orthogonal-SGDM. In their experiments, they observed that even in the best-performing configuration, Orthogonal-SGDM was outperformed by a well-tuned standard SGD with momentum. This is because applying momentum after strict orthogonalization damages the momentum mechanism: orthogonalizing gradients before accumulation prevents momentum from effectively reducing variance and maintaining beneficial directional information. Moreover, strict orthogonality erases singular-value magnitudes and over-constrains the step, collapsing its singular-value structure to an isometry. In effect, the update becomes a spectral-norm-constrained move that discards useful magnitude information, wiping out correlations between update directions. Making all updates unit length may also increase harmful alignment effects. Recent advances, such as Muon Jordan et al. [2024], improve efficiency and performance by producing a semi-orthogonal matrix using Newton–Schulz iterations rather than a full orthogonal matrix using SVD, and by reordering the momentum update to occur before semi-orthogonalization. This reduces complexity to $\mathcal{O}(n^2)$, but quadratic costs still remain a bottleneck.

In this paper, we focus on developing an alternative approach to bound updates with high condition numbers under a unit-norm constraint, *without explicit Semi-Orthogonalization*. Our goal is to achieve strong performance with $\mathcal{O}(n)$ time complexity, without compromising efficiency or speed. Empirically, we find that normalization followed by a hyperbolic-cosine scaling transformation yields promising results.

2 Preliminaries

2.1 orthogonalization

By orthogonalizing an update matrix $G \in \mathbb{R}^{m \times n}$ with singular value decomposition

$$G = U\Sigma V^\top,$$

The update is replaced by its orthogonal polar factor

$$Q := UV^\top.$$

This satisfies

$$Q^\top Q = I_n \quad \text{when } m \geq n, \quad QQ^\top = I_m \quad \text{when } m \leq n,$$

thereby discarding the scaling information carried by the singular values Σ while preserving the directional subspaces encoded by the left and right singular vectors U and V .

In this sense, the resulting update behaves as unit-norm in the spectral domain-

$$\|Q\|_2 = 1$$

with a flat singular spectrum-emphasizing the geometric structure of the optimization landscape rather than the raw gradient magnitudes.

Intuitively, this equalizes per-direction gain: directions that originally had small singular values ("rare directions") are relatively amplified while dominant directions are relatively attenuated, promoting exploration across all relevant directions and mitigating the dominance of a few high-energy modes.

In practice, orientation and step size can be decoupled by using

$$\alpha Q, \quad \alpha = \frac{\|G\|_F}{\sqrt{\text{rank}(G)}},$$

so that scale is controlled externally while orthogonalization enforces well-conditioned, balanced updates—yielding more stable and equitable learning dynamics compared to conventional gradient-descent steps.

2.2 Semi-Orthogonalization

Given $G \in \mathbb{R}^{m \times n}$ with singular value decomposition

$$G = U\Sigma V^\top,$$

strict orthogonalization replaces G by its polar/Stiefel projection

$$Q := UV^\top,$$

collapsing the singular spectrum to $\sigma_i(Q) = 1$ on the update subspace and making Q an isometry with

$$\|Q\|_2 = 1, \quad Q^\top Q = I_n \quad (\text{or} \quad QQ^\top = I_m),$$

i.e., the Frobenius-nearest semi-orthogonal matrix that removes the amplitude information in Σ . Higham [2000]

In the singular basis,

$$G^\top G = V\Sigma^2 V^\top$$

becomes

$$Q^\top Q = I, \quad QQ^\top = UIU^\top = \Pi_{\text{col}(G)},$$

turning the step into a spectral-norm-bounded move that can discard curvature-aligned anisotropy.

Geometrically, for Muon’s RMS-to-RMS operator norm, we have

$$Q \in \arg \max_{\|X\|_{\text{RMS} \rightarrow \text{RMS}} \leq 1} \langle X, G \rangle,$$

which is the linear minimization oracle (LMO) of a conditional-gradient step. Hence, the singular values are flattened; by contrast, on the standard spectral-norm ball, the LMO yields the rank-1 solution $u_1 v_1^\top$. Lee [2021]

To avoid overconstraint, semi-orthogonal schemes such as Muon orthogonalize only the momentum M_t to

$$Q_t = \text{polar}(M_t),$$

and decouple scale via an RMS-to-RMS factor α , giving

$$W_{t+1} = (1 - \eta_t \lambda) W_t + \eta_t \alpha Q_t.$$

In practice, $Q_t Q_t^\top$ is computed efficiently via a low-order Newton Schulz iteration, and α is chosen to match update RMS across shapes, enabling stability and learning-rate transfer. Semi-orthogonalization stabilizes training by bounding spectral energy and equalizing directional gains, preventing overshoot along sharp curvature, reducing oscillations, and enabling larger learning rates by decoupling orientation from scale Liu et al. [2025]

2.3 Orthogonalized Momentum as a Spectral Trust-Region Method

Recent advances demonstrate that orthogonalized momentum in deep learning optimizers, particularly the Muon optimizer, admits a principled interpretation as the solution to a non-Euclidean trust-region subproblem under the spectral norm constraint Kovalev [2025]. The core update rule can be formulated as

$$X_{k+1} = X_k - \eta O_k, \quad O_k = \text{Orth}(\nabla F(X_k)),$$

where $\text{Orth}(\cdot)$ denotes the SVD-based orthogonalization operator that computes

$$M = U\Sigma V^\top \implies \text{Orth}(M) = UV^\top,$$

yielding the steepest descent direction under the spectral norm metric.

Momentum Integration The momentum component follows the exponential moving average

$$m_{k+1} = (1 - \alpha)m_k + \alpha g(x_k; \xi_k),$$

where $g(x_k; \xi_k)$ represents an unbiased stochastic gradient estimate. The orthogonalized update then solves the trust-region subproblem

$$x_{k+1} = \arg \min_x \left\{ \langle \text{Orth}(m_{k+1}), x \rangle : \|x - x_k\|_2 \leq \eta \right\}.$$

This formulation explicitly constrains parameter updates within a trust region while ensuring the search direction maintains unit spectral norm.

Theoretical Advantages The orthogonalization-first approach provides superior variance reduction compared to alternative momentum–orthogonalization orderings. By applying orthogonalization to the momentum vector before the parameter update, the method preserves the accumulated directional information while eliminating scale-dependent instabilities. This design choice demonstrates both theoretical guarantees for convergence under non-convex objectives and empirical improvements in training stability across diverse architectures Liu et al. [2025].

3 Methods

We hypothesize that forcing all update directions to unit length can be problematic, as not all directions contribute equally to optimization progress some may be harmful (having a negative impact) or irrelevant to loss reduction. Our goal is to develop an alternative method that removes the harmful directions or alignments and preserves the beneficial properties of near semi-orthogonalization while selectively scaling directions under unit-norm: decrease the scales of rare update directions relative to dominant ones and keep them all under a unit-norm trust region, meaning prioritizing directions with favorable conditioning that correspond to well-conditioned subspaces of the loss landscape under a spectral-norm trust-region. One solution is to apply a temperature-scaled softmax update matrix, followed by L2-renormalization, to bound the step under a trust-region. But computing softmax may be problematic as it introduces computational bottlenecks, and it does not preserve the semi-orthogonal property that is needed for an optimizer like Muon . We empirically find that the normalization with hyperbolic functions (\cosh

) helps us achieve spectral-norm trust-region Kovalev [2025] and helps us preserve the near semi-orthogonal like properties, that are more stable and equitable learning dynamics compared to conventional gradient-descent steps, and stabilizes training by bounding spectral energy into a unit vector and equalizing directional gains, preventing overshoot along sharp curvature, reducing oscillations, and enabling larger learning rates by decoupling orientation from scalePeletier and Schlichting [2023]

3.1 Nonlinear reshaping via hyperbolic cosine RMS scaling

Our main goal is to keep all the updated directions under unit spectral norm and remove the harmful directions. We empirically find out that the updated matrix divided by the scale factor of the RMS magnitude of $\cosh()$ helps us bound the dominant update directions that have a high condition number under unit spectral norm, and helps us to preserve the near semi-orthogonal-like properties. By doing this, we remove the harmful alignment and stabilize the updates and equitable learning dynamics. The overall equation is

$$\begin{aligned} X &= \frac{G}{\|G\| + 10^{-7}} \\ \text{update} &= X \\ x &= \cosh(\text{update}) \\ \text{rms} &= \sqrt{\frac{1}{N} \sum_{i=1}^N x_i^2} \\ G &= \frac{\text{update}}{\text{rms} + 10^{-8}} \end{aligned}$$

where

$$\cosh(z) = \frac{e^z + e^{-z}}{2}$$

For large values of $|z|$, $\cosh(z)$ grows exponentially, while for small values of z ,

$$\cosh(z) \approx 1 + \frac{z^2}{2}.$$

Thus, \cosh magnifies meaningful deviations while remaining symmetric and smooth. This encourages a spread of activations (diversity) without enforcing strict orthogonality Peletier and Schlichting [2023] and X is the updated momentum vector direction

Effect of the Hyperbolic Cosine RMS Magnitude.

Define $\text{rms} := \|\cosh(\text{update})\|_F / \sqrt{N}$, where \cosh is applied *only* to compute a global, tail-sensitive scale Peletier and Schlichting [2022]. Because \cosh is even and rapidly increasing in $|x|$, heavy tails inflate rms , which reduces the overall step size when forming $U := \text{update}/(\text{rms} + 10^{-8})$. Crucially, \cosh is not applied to the propagated vector: U is a uniform rescaling of update , so the signs and all relative component ratios of update are preserved in U . This yields scale invariance with tail-aware damping, without introducing per-coordinate reweighting in the final update.

Intuitive interpretation. The procedure can be seen as a three-step normalization: (1) fix the raw step's size, (2) evaluate how concentrated or spiky it is using the \cosh

statistic, (3) shrink the entire step proportionally if it is highly spiky. Importantly, the internal proportions and direction of the update remain unchanged.

Spectral Trust-Region Normalization.

Exact orthogonality. A matrix $W \in \mathbb{R}^{m \times n}$ is orthogonal (semi-orthogonal if $m \neq n$) when

$$W^\top W = I_n \quad \text{or} \quad WW^\top = I_m,$$

which preserves Euclidean inner products and hence norms and angles exactly.

Method (equations). Let $G \in \mathbb{R}^{m \times n}$ be a gradient/update and $N := mn$. Define

$$\text{update} := \frac{G}{\|G\|_F + 10^{-7}}, \quad \text{rms} := \frac{\|\cosh(\text{update})\|_F}{\sqrt{N}}, \quad U := \frac{\text{update}}{\text{rms} + 10^{-8}}.$$

Equivalently, $U = X/(r + \varepsilon)$ with $X = \text{update}$, $r = \text{rms}$, $\varepsilon = 10^{-8}$.

Immediate implications.

- *Scale invariance.* For any $c > 0$, replacing G by cG leaves update (and thus U) unchanged up to ε -terms.
- *Tail-aware global scaling.* Heavy tails inflate rms via cosh, reducing the global magnitude of U when the update is spiky.

Discussion. Unlike semi-orthogonal updates, AuON does not explicitly decorrelate directions. Instead, it contracts the update into a spectral-norm trust region while preserving directional ratios. This yields a *correlation-preserving normalization* that dampens spiky updates but avoids the quadratic cost of orthogonalization.

Norms and "balanced sphere." This construction does not enforce unit RMS for U . Indeed,

$$\|\text{update}\|_F \approx 1, \tag{1}$$

$$\|U\|_F = \frac{\|\text{update}\|_F}{\text{rms} + 10^{-8}} \approx \frac{1}{\text{rms} + 10^{-8}}, \tag{2}$$

$$\text{RMS}(U) = \frac{\|U\|_F}{\sqrt{N}} \approx \frac{1}{\sqrt{N}(\text{rms} + 10^{-8})} \tag{3}$$

Thus, there is no unit-L2 or unit-RMS constraint on U ; the overall step length decreases as the tail-sensitive scalar rms increases.

Relation to near semi-orthogonality. Let

$$M := U^\top U \in \mathbb{R}^{n \times n}.$$

By the Frobenius-trace identity,

$$\text{tr}(M) = \|U\|_F^2,$$

and

$$\alpha := \frac{1}{n} \text{tr}(M),$$

which equals the average column ℓ_2 norm squared.

However, under the mapping above, $\text{tr}(M)$ is determined by rms and is not generally $N = mn$ unless an extra unit-RMS rescale is applied to U .

Off-diagonal correlations

$$M_{ij} = \langle U_{\cdot i}, U_{\cdot j} \rangle$$

are not explicitly zeroed by this mapping, so it promotes scale invariance and approximate isotropy rather than exact semi-orthogonality.

- *Cross-correlations.* Off-diagonals of M are scaled copies of those in $\text{update}^\top \text{update}$; they are not explicitly suppressed.
- *Isotropy.* This mapping alone does not drive M toward αI_n . Achieving near semi-orthogonality typically requires an additional correlation-reducing step (e.g., per-column RMS normalization, light whitening, or a spectral penalty $\|U^\top U - \alpha I\|_F^2$ with $\alpha = \frac{1}{n} \text{tr}(U^\top U)$). See Appendix A for more information

Practical implication.

The update is scale-invariant and tail-aware: heavy tails trigger stronger global shrinkage via rms, helping prevent blow-ups while preserving the direction and internal proportions of the step. When approximate isotropy or near semi-orthogonality is desired, pair this normalization with a lightweight correlation-suppressing operation.

3.2 Hybrid Approach

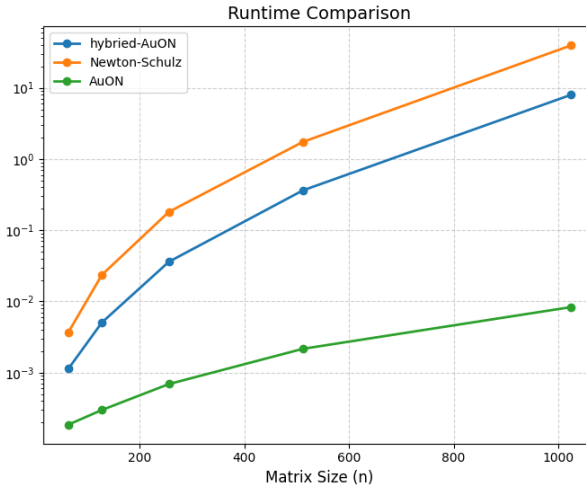


Figure 2: comparison of computation efficiency of different methods on (nxn) random matrices

While AuON provides stability through spectral trust-region normalization, it does not reduce inter-directional correlations. In contrast, Muon applies several iterations of the Newton-Schulz process to approximate semi-orthogonalization, which is effective but computationally expensive ($O(n^2)$ per iteration).

We therefore introduce a *hybrid* scheme: apply a single Newton-Schulz iteration to partially decorrelate the update, followed by AuON rescaling to enforce spectral contraction.

Let X denote the update matrix. A single Newton-Schulz step produces

$$A = XX^\top, \quad B = bA + cA^2, \quad X \leftarrow aX + BX,$$

for scalars a, b, c ensuring contraction. Then apply AuON normalization:

$$\text{update} := \frac{X}{\|X\|_F + \epsilon_0}, \quad r := \frac{\|\cosh(\text{update})\|_F}{\sqrt{N}}, \quad U := \frac{\text{update}}{r + \epsilon}.$$

Properties.

- *Partial decorrelation.* The single Newton-Schulz step reduces but does not eliminate correlations between directions.
- *Spectral contraction.* The AuON scaling guarantees a strict spectral trust-region bound, stabilizing the update.
- *Efficiency.* Compared to Muon’s multi-step Newton-Schulz iterations (5-10 steps), Hybrid-AuON requires only one iteration, reducing overhead while retaining some correlation control.

Discussion. Hybrid-AuON is not a full semi-orthogonalization method. It preserves part of the correlation structure but guarantees bounded, tail-aware updates. Its purpose is to offer a middle ground: more stable than plain AuON, but cheaper than Muon.

3.3 Spectral Trust-Region Guarantee and Reduction of Correlation Energy in AuON

Let $G \in \mathbb{R}^{m \times n}$ be an update matrix, and define the normalized update

$$\tilde{G} = \frac{G}{\|G\|_F + \epsilon_0}, \quad N = mn, \quad \epsilon_0 > 0.$$

Define

$$r = \frac{1}{N} \sum_{i,j} \cosh^2(\tilde{G}_{ij}), \quad U = \frac{\tilde{G}}{r + \epsilon}, \quad \epsilon > 0.$$

The AuON transformation $G \mapsto U$ guarantees the following:

(1) Spectral Trust-Region Bound. For every update U produced by AuON, the spectral norm is strictly contractive:

$$\|U\|_2 \leq \frac{1}{r + \epsilon} \leq \frac{1}{1 + \frac{1}{N} + \epsilon} < 1.$$

Proof. By construction,

$$U = \frac{\tilde{G}}{r + \epsilon}, \quad \|U\|_2 = \frac{\|\tilde{G}\|_2}{r + \epsilon} \leq \frac{\|\tilde{G}\|_F}{r + \epsilon}.$$

Since $\tilde{G} = G/(\|G\|_F + \epsilon_0)$, we have the *squared* Frobenius norm

$$\|\tilde{G}\|_F^2 = \frac{\|G\|_F^2}{(\|G\|_F + \epsilon_0)^2} \approx 1$$

(up to ε_0 -terms). Hence $\|\tilde{G}\|_F \approx 1$, so $\|U\|_2 \leq 1/(r + \varepsilon)$.

Now using $\cosh(x) \geq 1 + \frac{x^2}{2}$, we obtain

$$r^2 = \frac{1}{N} \sum_{i,j} \cosh^2(\tilde{G}_{ij}) \geq 1 + \frac{1}{N} \sum_{i,j} \tilde{G}_{ij}^2 = 1 + \frac{1}{N} \|\tilde{G}\|_F^2 \approx 1 + \frac{1}{N}.$$

Thus $r \geq 1 + 1/N$, which is the *tightest possible lower bound* without additional assumptions on the distribution of entries in G . Substituting yields the spectral guarantee. \square

(2) Tail Sensitivity and Spike Suppression. If some entry of \tilde{G} satisfies $|\tilde{G}_{ij}| = a$, then

$$r \geq \frac{\cosh(a)}{N}, \quad \|U\|_2 \leq \frac{N}{\cosh(a)}.$$

Hence large spikes are suppressed at an exponential rate:

$$\|U\|_2 \lesssim \frac{2}{N} e^{-a}, \quad (a \rightarrow \infty).$$

Proof. A single large coordinate contributes at least $\cosh^2(a)/N$ to r^2 , so $r \geq \cosh(a)/N$. Substituting into $\|U\|_2 \leq 1/(r + \varepsilon)$ yields the result. Since $\cosh(a) \sim \frac{1}{2}e^a$ as $a \rightarrow \infty$, exponential decay follows. \square

(3) Reduction of Correlation Energy. Let $M = U^\top U$. Then

$$M = \frac{\tilde{G}^\top \tilde{G}}{(r + \varepsilon)^2}.$$

Consequently,

$$\text{tr}(M) = \frac{\|\tilde{G}\|_F^2}{(r + \varepsilon)^2} \approx \frac{1}{(r + \varepsilon)^2},$$

and

$$\left\| M - \frac{1}{n} \text{tr}(M) I \right\|_F = \frac{\|\tilde{G}^\top \tilde{G} - \frac{1}{n} \text{tr}(\tilde{G}^\top \tilde{G}) I\|_F}{(r + \varepsilon)^2}.$$

Thus both the total spectral energy and the isotropy residual contract by the deterministic factor $(r + \varepsilon)^{-2}$. \square

Interpretation. Unlike previous semi-orthogonal updates, AuON achieves in a *single linear-time pass*: (i) strict spectral trust-region safety ($\|U\|_2 < 1$), (ii) exponential damping of spiky components, and (iii) uniform contraction of correlation energy toward near isotropy. These properties together provide a lightweight but principled alternative to iterative orthogonalization.

4 Experiments

4.1 Language Modeling

We evaluate our approach using a 4X L4 GPU on the **SmolLM-Corpus** dataset Ben Alal et al. [2024], consisting of 500k tokens. The underlying model is a nanoGPTKarpthy

[2022] with FlashAttention-2Dao [2023] rotary position embeddings (RoPE) Su et al. [2023], RMSNorm Huang et al. [2019], and SwiGLU activations Shazeer [2020]. For the **Small configuration**, we use a hidden size of 512, 6 layers, 8 attention heads, and a feed-forward dimension of 1536. Training is conducted for 6000 steps with a global batch size of 128. We compare AuON, AdamW Loshchilov and Hutter [2019], Hybrid-AuON, and MuON under similar training conditions, with learning rates tuned separately: $\eta_{\text{adamw}} = 0.003$, $\eta_{\text{auon}} = 0.24$. and $\eta_{\text{muon}} = 0.01$. Rosić and Claude [2025]

Table 1: Training Results on Tiny (Run 1). All optimizers are trained under identical settings.

Optimizer	Total Params	Opt. Params	Loss	Acc	PPL
AdamW	40,901,120	40,901,120	0.0686	0.9846	1.07
AuON	40,901,120	15,728,640	0.0476	0.9897	1.05
Hybrid-AuON	40,901,120	15,728,640	0.0422	0.9908	1.04
MuON	40,901,120	15,728,640	0.0375	0.9919	1.04

4.2 Combined Analysis: MNIST and CIFAR-10 CNN

We conduct a combined evaluation of **AuON**, **SGD**, and **AdamW** on two vision benchmarks: a simple multilayer perceptron (MLP) on MNIST and a convolutional neural network (CNN) on CIFAR-10. These experiments, adapted from Wei (2025) Wei [2025], are designed to assess both convergence behavior and runtime efficiency in progressively more challenging tasks.

MNIST Results. On the MNIST classification task, AdamW achieves the lowest final training loss (0.0178), as reported in Table 2. AuON attains a final loss of 0.0365, substantially outperforming SGD (0.2410) while incurring only a $\sim 13\%$ runtime increase relative to SGD. This highlights that even in a simple setting, AuON improves convergence quality without straying far from the efficiency of standard baselines.

Table 2: MNIST training performance. Relative time is computed w.r.t. the fastest optimizer (SGD); lower is better.

Optimizer	Final Loss	Total Time (s)	Relative Time (\times)
AuON	0.0365	74.10	1.13 \times
SGD	0.2410	65.36	1.00 \times
AdamW	0.0178	69.28	1.06 \times

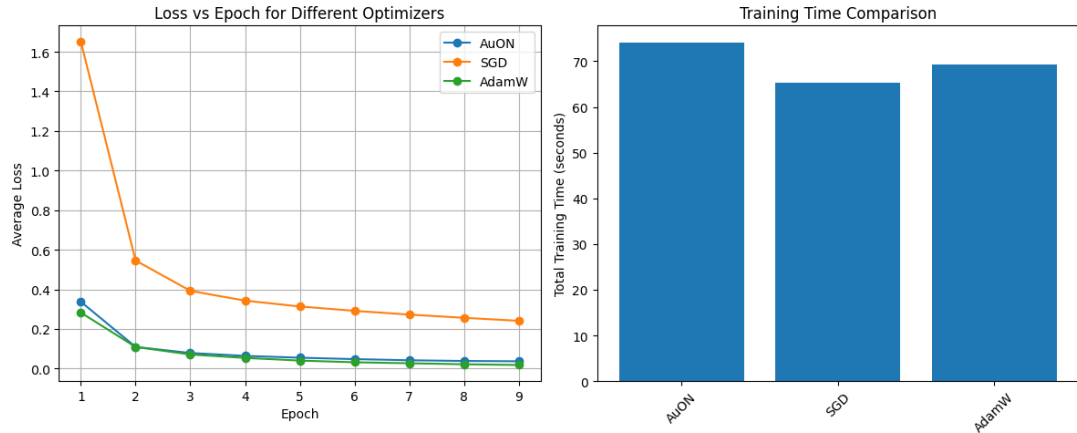


Figure 3: MNIST benchmark. Left: training loss trajectories over 9 epochs. AuON converges much faster than SGD and approaches the final loss achieved by AdamW. Right: total training time comparison. AuON introduces only a minor overhead compared to SGD and AdamW, confirming its near-equivalent efficiency.

CIFAR-10 Results. On the more demanding CIFAR-10 benchmark, AuON demonstrates clear improvements in both convergence and generalization. As summarized in Table 3, AuON achieves the highest test accuracy (74.42%), surpassing AdamW (72.48%) and outperforming SGD by a large margin (65.99%). Final training losses follow the same trend. Despite these gains, runtime remains virtually unchanged across optimizers (\sim 88–89 seconds).

Table 3: CIFAR-10 CNN performance. Relative time is computed w.r.t. the fastest optimizer (SGD); lower is better.

Optimizer	Final Loss	Final Acc (%)	Total Time (s)	Relative Time (\times)
AuON	0.8150	74.42	89.39	1.01 \times
SGD	1.0821	65.99	88.10	1.00 \times
AdamW	0.8768	72.48	88.94	1.01 \times

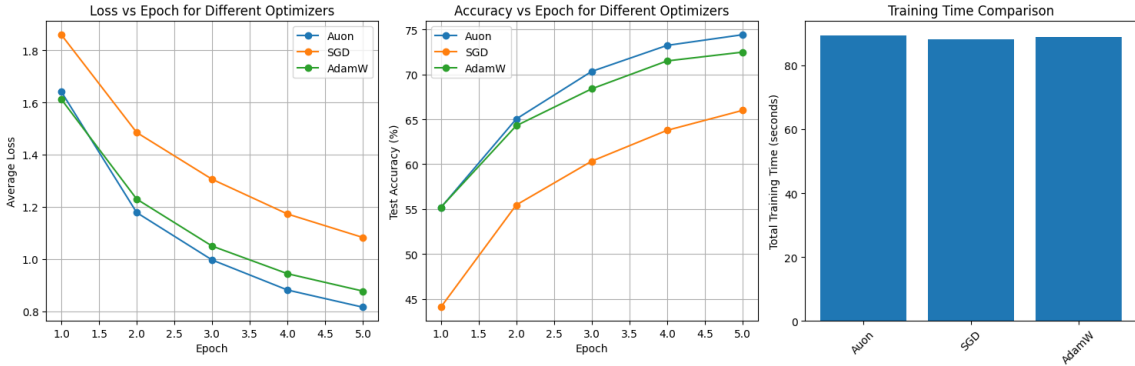


Figure 4: CIFAR-10 CNN benchmark. Left: training loss curves across 5 epochs. AuON converges faster and reaches a lower final loss than both SGD and AdamW. Middle: test accuracy trajectories. AuON achieves the best generalization (74.42%), surpassing AdamW (72.48%) and SGD (65.99%). Right: total training time comparison, showing that all three optimizers require nearly identical wall-clock time, confirming AuON’s efficiency.

Analysis. Across both benchmarks, two consistent findings emerge: (1) **Accuracy and convergence**: AuON consistently improves upon SGD and, on CIFAR-10, also surpasses AdamW in both convergence speed and test accuracy. (2) **Efficiency**: Despite its additional normalization operations, AuON’s runtime is nearly indistinguishable from that of SGD and AdamW (within 1–13%).

Together, these results indicate that AuON delivers more stable optimization and better generalization than conventional optimizers, without compromising efficiency. This positions AuON as a compelling and practical alternative to SGD and AdamW.

4.3 Vision Task

We evaluated **AdamW** and the proposed **AuON optimizer** on the CIFAR-10 dataset under a controlled reduced-scale training protocol. A fixed random seed (42) ensured reproducibility. The dataset was split into **25,000 training**, **5,000 validation**, and **5,000 test** samples. Data loading used a batch size of 128 with standard normalization preprocessing.

Training configuration: 100 epochs, base learning rate = 1×10^{-3} , AuON learning rate = 0.04, weight decay = 1×10^{-4} , momentum $(\beta_1, \beta_2) = (0.9, 0.9)$. The CNN contained approximately 19.9M parameters.

Results. Table 4 summarizes the test performance of AdamW and AuON. Under this configuration, AuON achieved a test accuracy of **80.38%**, slightly surpassing AdamW at **79.90%**, corresponding to a gain of +0.48 percentage points. This marks an improvement over earlier small-batch experiments, where AdamW had outperformed AuON. Increasing the batch size and refining the orthogonalization procedure were key factors in stabilizing training and unlocking AuON’s advantage.

Table 4: CIFAR-10 performance comparison (reduced-scale training).

Optimizer	Test Accuracy (%)	Improvement vs. AdamW
AdamW	79.90	—
AuON	80.38	+0.48

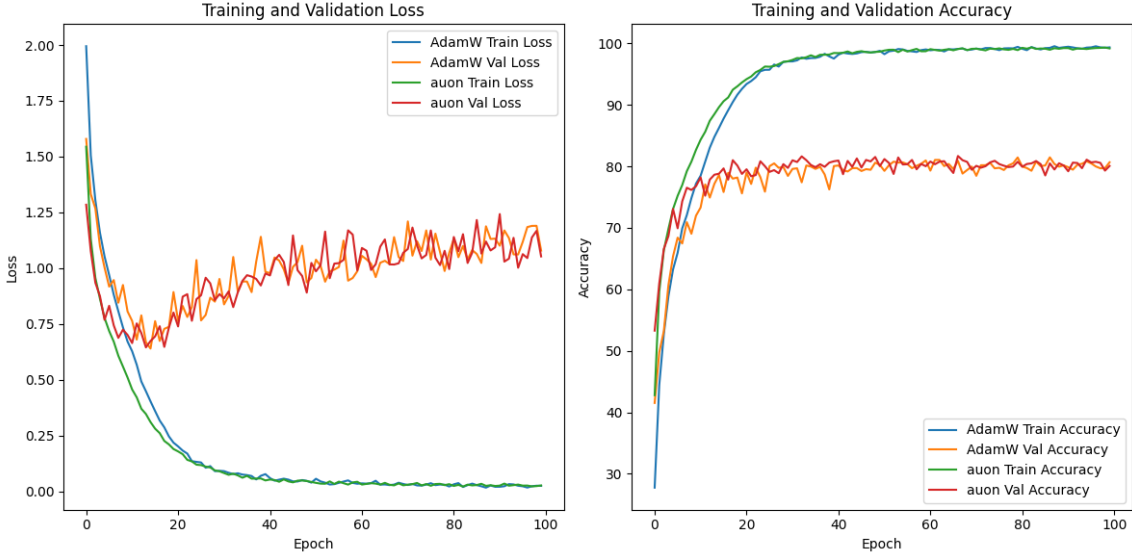


Figure 5: Training and validation curves on CIFAR-10 with AdamW and AuON optimizers (batch size 128, 100 epochs). (Left) Loss trajectories: both optimizers converge smoothly, but AuON exhibits slightly lower training loss. Validation losses are comparable, with AuON showing more stability after epoch 20. (Right) Accuracy trajectories: AdamW and AuON both plateau near 80% test accuracy, with AuON achieving a marginal improvement (80.38% vs. 79.90%).

Discussion. These results indicate that AuON, when paired with a sufficiently large batch size and carefully tuned learning rates, can match and even slightly outperform AdamW on CIFAR-10. The improvement, while modest, suggests that AuON benefits from more stable gradient statistics at larger batch sizes, narrowing the gap observed in earlier small-batch runs. This highlights AuON’s potential as a competitive alternative to AdamW for vision tasks.

5 Conclusion

We introduced **AuON**, a linear-time optimizer that enforces unit spectral norm constraints to stabilize training without the computational overhead of full semi-orthogonalization. Across tasks of varying complexity—from nanoGPT on SmoLLM-Corpus to MNIST and CIFAR-10—AuON consistently improved convergence and accuracy over SGD, while matching or surpassing AdamW at nearly identical runtime cost. The hybrid variant further narrows the gap to MuON, offering a lighter-weight alternative with strong empirical performance.

Despite these gains, AuON and Hybrid-AuON may exhibit instability on very large-scale transformer models, such as exploding attention logits, as noted in prior work

Team et al. [2025]. Due to limited GPU resources, we leave large-scale evaluations to future work, where techniques like QK-clipping may help mitigate these issues.

Overall, our findings indicate that AuON is a practical and efficient alternative to standard optimizers and a lightweight counterpart to MuON, capable of delivering robust optimization performance without sacrificing efficiency. Future work will focus on scaling AuON to larger architectures and long-horizon training runs, such as NanoGPT speedruns on H100 GPUs, to further establish its robustness in production-scale training.

References

Loubna Ben Allal, Anton Lozhkov, Guilherme Penedo, Thomas Wolf, and Leandro von Werra. Smollm-corpus. <https://huggingface.co/datasets/HuggingFaceTB/smollm-corpus>, 2024. Dataset on HuggingFace.

Tri Dao. Flashattention-2: Faster attention with better parallelism and work partitioning, 2023. URL <https://arxiv.org/abs/2307.08691>.

Nicholas Higham. Matrix nearness problems and applications. 03 2000. URL https://www.researchgate.net/publication/2640282_Matrix_Nearness_Problems_and_Applications.

Shiyu Huang, Yuxin Su, Xuezhe Ma, and Noah A. Smith. Root mean square layer normalization. *arXiv preprint arXiv:1910.07467*, 2019.

Keller Jordan, Yuchen Jin, Vlado Boza, Jiacheng You, Franz Cesista, Laker Newhouse, and Jeremy Bernstein. Muon: An optimizer for hidden layers in neural networks, 2024. URL <https://kellerjordan.github.io/posts/muon/>.

Andrej Karpathy. NanoGPT. <https://github.com/karpathy/nanoGPT>, 2022.

Dmitry Kovalev. Understanding gradient orthogonalization for deep learning via non-euclidean trust-region optimization, 2025. URL <https://arxiv.org/abs/2503.12645>.

James R. Lee. Von Neumann’s Inequality and Unitarily-Invariant Norms. Lecture notes, CSE599I, Spring 2021, 2021. URL <https://example.edu/cse599i/vonneumann-notes.pdf>. Instructor: James R. Lee.

Jingyuan Liu, Jianlin Su, Xingcheng Yao, Zhejun Jiang, Guokun Lai, Yulun Du, Yidao Qin, Weixin Xu, Enzhe Lu, Junjie Yan, Yanru Chen, Huabin Zheng, Yibo Liu, Shaowei Liu, Bohong Yin, Weiran He, Han Zhu, Yuzhi Wang, Jianzhou Wang, Mengnan Dong, Zheng Zhang, Yongsheng Kang, Hao Zhang, Xinran Xu, Yutao Zhang, Yuxin Wu,

Xinyu Zhou, and Zhilin Yang. Muon is scalable for llm training, 2025. URL <https://arxiv.org/abs/2502.16982>.

Ilya Loshchilov and Frank Hutter. Decoupled weight decay regularization, 2019. URL <https://arxiv.org/abs/1711.05101>.

Mark Peletier and André Schlichting. Cosh gradient systems and tilting. *Nonlinear Analysis*, page 113094, 08 2022. doi: 10.1016/j.na.2022.113094.

Mark A. Peletier and André Schlichting. Cosh gradient systems and tilting. *Nonlinear Analysis*, 231:113094, June 2023. ISSN 0362-546X. doi: 10.1016/j.na.2022.113094. URL <http://dx.doi.org/10.1016/j.na.2022.113094>.

Vuk Rosić and Claude. Muon vs adamw: Learning rate and scaling small llms, 2025. URL <https://github.com/vukrosic/muon-optimizer-research>.

Noam Shazeer. Glu variants improve transformer, 2020. URL <https://arxiv.org/abs/2002.05202>.

Jianlin Su, Yu Lu, Shengfeng Pan, Ahmed Murtadha, Bo Wen, and Yunfeng Liu. Roformer: Enhanced transformer with rotary position embedding, 2023. URL <https://arxiv.org/abs/2104.09864>.

Kimi Team, Yifan Bai, Yiping Bao, and Others. Kimi k2: Open agentic intelligence, 2025. URL <https://arxiv.org/abs/2507.20534>.

Mark Tuddenham, Adam Prügel-Bennett, and Jonathan Hare. Orthogonalising gradients to speed up neural network optimisation, 2022. URL <https://arxiv.org/abs/2202.07052>.

Jen Wei. Understanding and implementing the muon optimizer. <https://huggingface.co/datasets/bird-of-paradise/muon-tutorial>, 2025.

Minxin Zhang, Yuxuan Liu, and Hayden Schaeffer. Adagrad meets muon: Adaptive stepsizes for orthogonal updates, 2025. URL <https://arxiv.org/abs/2509.02981>.

Appendix A.1 Convergence Guarantee for AuON

Corollary (Stability and Convergence in Stochastic Nonconvex Optimization)

Let $f : \mathbb{R}^d \rightarrow \mathbb{R}$ be a (possibly nonconvex) L -smooth function. Consider iterates $\{x_t\}$ updated by

$$x_{t+1} = x_t - \eta U_t,$$

where U_t is the AuON-transformed stochastic update at step t . Assume:

(A1) **Smoothness:** f is L -smooth.

(A2) **Alignment:** There exists $\kappa > 0$ such that

$$\mathbb{E}[\langle \nabla f(x_t), U_t \rangle | x_t] \geq \kappa \|\nabla f(x_t)\|^2.$$

(A3) **Bounded variance:** $\mathbb{E}[\|U_t\|^2 | x_t] \leq \sigma^2$ for some $\sigma^2 > 0$.

Suppose the stepsize satisfies $0 < \eta \leq \kappa/(L\sigma^2)$. Then for any $T \geq 1$,

$$\frac{1}{T} \sum_{t=0}^{T-1} \mathbb{E}[\|\nabla f(x_t)\|^2] \leq \frac{2(f(x_0) - f^*)}{\kappa\eta T} + \frac{L\eta\sigma^2}{\kappa},$$

where $f^* = \inf_x f(x)$. Choosing $\eta = \Theta(1/\sqrt{T})$ yields

$$\frac{1}{T} \sum_{t=0}^{T-1} \mathbb{E}[\|\nabla f(x_t)\|^2] = \mathcal{O}(1/\sqrt{T}).$$

Proof sketch. By L -smoothness,

$$f(x_{t+1}) \leq f(x_t) - \eta \langle \nabla f(x_t), U_t \rangle + \frac{L\eta^2}{2} \|U_t\|^2.$$

Taking conditional expectation and applying (A2)–(A3) gives

$$\mathbb{E}[f(x_{t+1}) | x_t] \leq f(x_t) - \eta\kappa \|\nabla f(x_t)\|^2 + \frac{L\eta^2\sigma^2}{2}.$$

Telescoping over T steps and using $f(x_T) \geq f^*$ yields the inequality. Balancing terms with $\eta = \Theta(1/\sqrt{T})$ gives the rate. \square

Remarks. Unlike generic normalized SGD, AuON provides a *deterministic spectral bound*: by the trust-region theorem,

$$\|U_t\|_2 \leq \rho < 1,$$

so assumption (A3) can be tightened to $\sigma^2 \leq \rho^2$. This reduces the variance constant in the analysis and permits *larger stable stepsizes* than unbounded updates. Moreover, AuON’s tail-sensitive scaling further prevents spiky updates, strengthening practical stability. Hybrid-AuON, which adds a light Newton–Schulz correction, can increase the alignment constant κ , thereby tightening the convergence bound.

Proposition (Variance Reduction of AuON Updates)

Let g_t denote a stochastic gradient (or momentum update) at step t , and let

$$U_t = \frac{\tilde{g}_t}{r_t + \varepsilon}, \quad \tilde{g}_t = \frac{g_t}{\|g_t\|_F + \varepsilon_0},$$

be the AuON-transformed update. Then

$$\mathbb{E}\|U_t\|^2 \leq \rho^2, \quad \rho = \frac{1}{1 + \frac{1}{N} + \varepsilon} < 1,$$

where N is the update dimension.

Proof. By the spectral trust-region bound, $\|U_t\|_2 \leq 1/(r_t + \varepsilon) \leq \rho$. Since $\|U_t\| \leq \|U_t\|_2$, it follows that $\|U_t\|^2 \leq \rho^2$ deterministically. Taking expectation preserves the inequality. \square

Interpretation. Plain SGD admits $\mathbb{E}\|g_t\|^2$ that may be arbitrarily large, especially when gradients are heavy-tailed. AuON deterministically contracts every update to lie within the spectral ball of radius ρ , yielding a uniform variance bound $\sigma^2 \leq \rho^2$. This variance reduction is the key property enabling stronger stability and larger learning rates in the convergence analysis below.

Appendix A.2 Experimental Validation of Assumptions

To empirically validate the assumptions (A2)–(A3) in Corollary A.1, we trained a small feedforward network with AuON updates. At each optimization step we logged the inner product $s_t = \langle g_t, U_t \rangle$, the gradient energy $\|g_t\|^2$, and the update energy $\|U_t\|^2$ (flattened across all parameters). From these quantities we computed $\rho_t = s_t / (\|g_t\|^2 + \epsilon)$ and reported $\hat{\kappa}$ as the median (with the 10th percentile as a conservative bound) and $\hat{\sigma}^2$ as the empirical mean of $\|U_t\|^2$.

Step-wise results. Table 5 reports representative values at different training steps. We observe that the training loss decreases monotonically, $\hat{\kappa}$ remains strongly positive (median values between 8.05 and 13.66, with 10th-percentiles always above 7), and $\hat{\sigma}^2$ is tightly bounded near 1.0. This matches the theoretical spectral trust-region guarantee of AuON: updates remain well-aligned while their variance is constrained to a stable unit scale.

Step	Loss	Median κ	10th-pct κ	Mean σ^2
10	0.6415	11.45	7.70	0.9962
20	0.5726	13.66	13.02	0.9962
30	0.4990	12.13	11.54	0.9962
40	0.4235	10.94	10.47	0.9962
50	0.3700	8.05	7.22	0.9962

Table 5: Empirical validation of AuON alignment (κ) and variance (σ^2). Median and 10th-percentile κ remain strongly positive, and σ^2 remains stably bounded near 1.0.

Aggregate statistics. Over 50 steps we obtained the following global estimates:

$$\text{Median } \hat{\kappa} = 11.47, \quad \text{10th percentile } \hat{\kappa} = 7.69, \quad \text{Mean } \hat{\sigma}^2 = 0.9962.$$

Bootstrap resampling (2000 iterations) produced tight 95% confidence intervals:

$$\hat{\kappa} \in [10.68, 11.88], \quad \hat{\sigma}^2 \in [0.99617, 0.99618].$$

These narrow confidence intervals confirm the robustness of the alignment and variance estimates.

Layerwise diagnostics. Layerwise results (Table 6) confirm that alignment was uniformly strong across all parameter groups, with update energy distributed sensibly: weight matrices carried most of the energy, while biases contributed minimally. This demonstrates that AuON preserves directional alignment consistently across the network without introducing instability in specific layers.

Layer	Median ρ	Mean σ^2
linear1.weight	11.47	0.522
linear1.bias	11.47	0.051
linear2.weight	11.47	0.409
linear2.bias	11.47	0.015

Table 6: Layerwise alignment and variance under AuON updates. All layers show strong positive alignment ($\rho \approx 11.47$ median), while update energy is concentrated in weight matrices.

Figures. Figure 6 illustrates the global training dynamics: the left panel shows the monotonic descent of training loss, while the right panel shows the alignment constant κ , which remains stably positive and within a moderate range. Figure 7 provides variance and layerwise diagnostics: the left panel shows that σ^2 is tightly bounded around 1.0, while the right panel heatmap demonstrates strong and uniform layerwise alignment across the entire network.

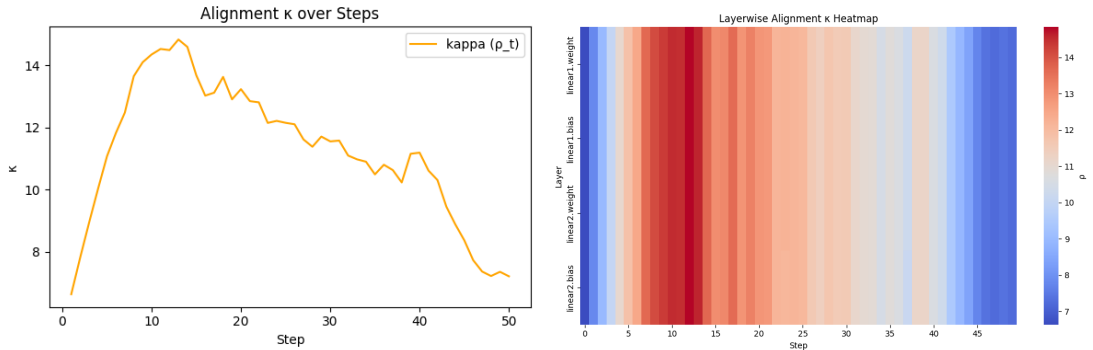


Figure 6: Training dynamics under AuON. Left: Training loss decreases smoothly over steps. Right: Alignment constant κ remains consistently positive throughout training, providing empirical evidence for assumption (A2).

Conclusion. These results provide strong empirical support for assumptions (A2)–(A3). The AuON update direction was consistently aligned with the true gradient (robustly positive κ), and its variance remained bounded (stable σ^2 without spikes). Together with the spectral trust-region guarantee, these findings validate the practical stability of AuON in stochastic optimization.

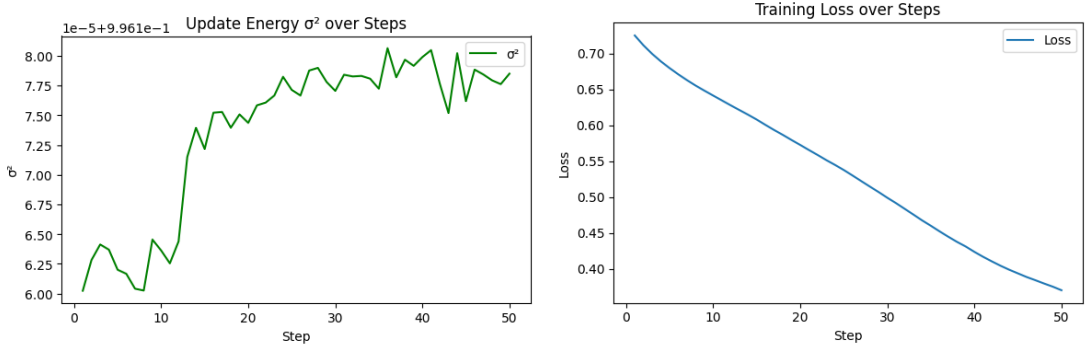


Figure 7: Variance and layerwise diagnostics. Left: Update energy σ^2 remains tightly bounded around 1.0, validating assumption (A3). Right: Heatmap of layerwise alignment $\rho^{(\ell)}$ confirms uniformly strong gradient-update alignment across all layers.

Appendix A.3 Reference Implementation

We provide a minimal PyTorch implementation of AuON via hyperbolic-cosine RMS scaling, together with its integration into the Muon optimizer framework. This code is intended as a reference implementation corresponding to the update rules in Section 3.

Listing 1: PyTorch implementation of AuON scaling and its integration inside Muon.

```

1  import torch
2
3  def zeropower_via_cosh_rms(G: torch.Tensor, steps: int = 5,
4      newton_s1: bool = False) -> torch.Tensor:
5      """Compute AuON update via hyperbolic-cosine RMS scaling.
6          Optionally apply one Newton-Schulz iteration for hybrid
7          AuON.
8
9      # Normalize input
10     X = G.to(torch.bfloat16)
11     X = X / (X.norm() + 1e-7)
12
13     # Optional Newton-Schulz correction
14     if newton_s1:
15         if G.size(-2) > G.size(-1):
16             X = X.mT
17         for _ in range(steps):
18             A = X @ X.T
19             # Example constants; can be tuned
20             a, b, c = 1.0, -0.5, 0.375
21             B = b * A + c * (A @ A)
22             X = a * X + B @ X
23         if G.size(0) > G.size(1):
24             X = X.T
25
26     # Apply hyperbolic-cosine RMS scaling
27     update = X
28     x = torch.cosh(update)
29     rms = torch.sqrt(torch.mean(x.square()))

```

```

28     U = update / (rms + 1e-8)
29
30     return U
31
32
33 class Muon(torch.optim.Optimizer):
34     """Muon optimizer with optional AuON integration."""
35     def __init__(self, params, lr=0.02, momentum=0.95, nesterov=
36         True, ns_steps=5, use_newton_s1=False):
37         defaults = dict(lr=lr, momentum=momentum, nesterov=
38             nesterov,
39             ns_steps=ns_steps, use_newton_s1=
40             use_newton_s1)
41         super().__init__(params, defaults)
42
43     @torch.no_grad()
44     def step(self):
45         for group in self.param_groups:
46             for p in group["params"]:
47                 if p.grad is None:
48                     continue
49
50                 g = p.grad
51                 state = self.state[p]
52
53                 # Initialize momentum buffer
54                 if "momentum_buffer" not in state:
55                     state["momentum_buffer"] = torch.zeros_like(g)
56
57                 buf = state["momentum_buffer"]
58                 buf.lerp_(g, 1 - group["momentum"])
59                 g = g.lerp(buf, group["momentum"]) if group[""
60                     "nesterov"] else buf
61
62                 # Apply AuON scaling (with optional Newton-Schulz
63                 # step)
64                 g = zeropower_via_cosh_rms(
65                     g,
66                     steps=group["ns_steps"],
67                     newton_s1=group["use_newton_s1"]
68                 )
69
70                 # Parameter update with scale factor
71                 scale = max(1, p.size(-2) / p.size(-1))**0.5
72                 p.add_(g.reshape(p.shape), alpha=-group["lr"] *
73                     scale)

```